



ANP-10320NP
Revision 0

Summary Report on Postirradiation Examinations of MOX Fuel

February 2012

AREVA NP Inc.

Copyright © 2012
AREVA NP Inc.
All Rights Reserved

This page intentionally left blank

Nature of Changes

| Item | Section(s) or Page(s) | Description and Justification |
|--------|--------------------------|-------------------------------|
| Rev. 0 | all | Initial release. |

Contents

| | <u>Page</u> |
|--|-------------|
| 1.0 INTRODUCTION..... | 1-1 |
| 1.1 Scope and Extent of Examinations | 1-2 |
| 1.2 Organization of Report | 1-2 |
| 2.0 SUMMARY AND CONCLUSIONS..... | 2-1 |
| 3.0 RESULTS OF POOLSIDE EXAMINATIONS | 3-1 |
| 3.1 Fuel Assembly Visual Examinations..... | 3-1 |
| 3.2 Fuel Rod Visual Examinations (Poolside) | 3-2 |
| 3.3 Fuel Assembly Growth | 3-2 |
| 3.4 Fuel Rod Growth (Poolside Measurements) | 3-3 |
| 3.5 Fuel Assembly Bow..... | 3-5 |
| 3.6 Spacer Grid Width..... | 3-6 |
| 3.7 Fuel Rod Oxide Thickness | 3-7 |
| 3.8 Water Channels..... | 3-8 |
| 3.9 Guide Thimble Oxide Thickness..... | 3-9 |
| 3.10 Holddown Spring Height..... | 3-10 |
| 3.11 Holddown Spring Stiffness | 3-10 |
| 4.0 RESULTS OF HOT CELL EXAMINATIONS..... | 4-12 |
| 4.1 Fuel Rod Visual Examinations (Hot Cell) | 4-12 |
| 4.2 Fuel Rod Growth (Hot Cell Measurements) | 4-13 |
| 4.3 Gamma Scanning..... | 4-14 |
| 4.4 Eddy Current Testing | 4-19 |
| 4.5 Fuel Rod Profilometry..... | 4-19 |
| 4.6 Gas Pressure, Void Volume, and Gas Analysis | 4-24 |
| 4.7 Optical Microscopy of Fuel and Cladding | 4-28 |
| 4.8 Transmission Electron Microscopy of Cladding..... | 4-30 |
| 4.9 Scanning Electron Microscopy of Fuel and Cladding, Radial Burnup Profile ... | 4-31 |
| 4.10 Burnup Determination | 4-34 |
| 4.11 Isotopic Analysis of Fuel..... | 4-35 |
| 4.12 Gallium Analysis..... | 4-43 |
| 4.13 Cladding Hydrogen Analysis | 4-44 |
| 4.14 Mechanical Testing of Cladding: Expanding Plug | 4-46 |
| 4.15 Mechanical Testing of Cladding: Axial Tensile..... | 4-46 |
| 4.16 Pellet Density | 4-46 |
| 4.17 Inspection of Wear Marks..... | 4-47 |
| 4.18 Cladding Surface Microscopy..... | 4-48 |
| 5.0 REFERENCES..... | 5-1 |

List of Tables

Table 1-1—Extent of Hot Cell Examinations..... 1-4

Table 1-2—Applicability of Examination Results to SRP In-Reactor Phenomena..... 1-5

Table 4-1—Comparison of Measured and Calculated Gas Pressures 4-26

Table 4-2—Calculated Gas Pressure for Rod C-01 with Increased Burnup..... 4-26

Table 4-3—Hydrogen Concentrations for Irradiated Cladding..... 4-45

Table 4-4—Fractional Density of Irradiated Fuel 4-47

List of Figures

| | |
|---|------|
| Figure 1-1—General Arrangement of Mark-BW/MOX1 Lead Assembly | 1-6 |
| Figure 1-2—Locations of Rods Selected for Hot Cell Examination | 1-7 |
| Figure 3-1—Comparison of MOX Fuel Rod Growth with Experience | 3-5 |
| Figure 4-1—Low-Energy Gamma Scan for Rod A-01 | 4-17 |
| Figure 4-2—Low-Energy Gamma Scan for Rod B-04 | 4-17 |
| Figure 4-3—Low-Energy Gamma Scan for Rod B-14 | 4-18 |
| Figure 4-4—Low-Energy Gamma Scan for Rod C-01 | 4-18 |
| Figure 4-5—Low-Energy Gamma Scan for Rod K-05 | 4-19 |
| Figure 4-6—Measured and Predicted Diameter Profiles for Rod A-01 | 4-22 |
| Figure 4-7—Measured and Predicted Diameter Profiles for Rod B-04 | 4-22 |
| Figure 4-8—Measured and Predicted Diameter Profiles for Rod B-14 | 4-23 |
| Figure 4-9—Measured and Predicted Diameter Profiles for Rod C-01 | 4-23 |
| Figure 4-10—Measured and Predicted Diameter Profiles for Rod K-05 | 4-24 |
| Figure 4-11—Measured and Predicted Void Volumes | 4-27 |
| Figure 4-12—Measured and Predicted Gas Pressures | 4-27 |
| Figure 4-13—Measured and Predicted Burnups | 4-35 |
| Figure 4-14—Measured and Calculated Uranium Concentrations | 4-37 |
| Figure 4-15—Measured and Calculated Plutonium Concentrations | 4-38 |
| Figure 4-16—Measured ²³³ U Abundances | 4-38 |
| Figure 4-17—Measured and Calculated ²³⁴ U Abundances | 4-39 |
| Figure 4-18—Measured and Calculated ²³⁵ U Abundances | 4-39 |
| Figure 4-19—Measured and Calculated ²³⁶ U Abundances | 4-40 |
| Figure 4-20—Measured and Calculated ²³⁸ U Abundances | 4-40 |
| Figure 4-21—Measured and Calculated ²³⁸ Pu Abundances | 4-41 |
| Figure 4-22—Measured and Calculated ²³⁹ Pu Abundances | 4-41 |
| Figure 4-23—Measured and Calculated ²⁴⁰ Pu Abundances | 4-42 |
| Figure 4-24—Measured and Calculated ²⁴¹ Pu Abundances | 4-42 |
| Figure 4-25—Measured and Calculated ²⁴² Pu Abundances | 4-43 |

Nomenclature

| Acronym | Definition |
|-----------------|---|
| ADEPT | Advanced Diagnostics and Evaluation Platform |
| DOE | Department of Energy |
| FR | fuel rod |
| GWd/MThm | gigawatt-days per metric ton of heavy metal |
| IHM | initial heavy metal |
| LEU | low-enriched uranium |
| M5 [®] | designation for an advanced cladding alloy |
| MOX | mixed oxide – uranium dioxide and plutonium dioxide |
| MSMG | mid-span mixing grid |
| PIE | post-irradiation examination |
| SRP | Standard Review Plan |
| UNS | Unified Numbering System (for metals and alloys) |
| WG | weapons-grade |

ABSTRACT

The U.S. Department of Energy is implementing a program to dispose of a portion of the nation's surplus weapons-grade plutonium by reconstituting the plutonium into mixed oxide fuel pellets and irradiating the fuel in commercial light water reactors. Accordingly, the Department of Energy has contracted with Shaw AREVA MOX Services to qualify the fuel for batch irradiation.

The qualification process includes irradiation of lead assemblies and both poolside and hot-cell post-irradiation examination of those assemblies. This report summarizes the results of all the examinations and discusses how they compare with predictions and expectations.

Four Mark-BW/MOX1 lead assemblies were supplied to Duke Energy's Catawba Nuclear Station, Unit 1, for irradiation starting in spring 2005. The assemblies were placed in high power but non-limiting locations that are expected to be representative of the batch peaking requirements. The first cycle of irradiation was completed in fall 2006, and the lead assemblies were examined at poolside. The second cycle was completed in spring 2008, and the assemblies were again examined at poolside. After the poolside examination, five fuel rods were removed from one assembly and shipped to Oak Ridge National Laboratory for hot cell examination. Together, the examination campaigns satisfy the requirements for postirradiation examination and the commitments for fuel qualification.

The examinations covered many aspects of fuel performance, some of which were specific to the Mark-BW/MOX1 fuel assembly design. It was found that (1) the fuel provided acceptable performance, (2) future irradiations may benefit from more advanced neutronic methods that will reduce the uncertainty for peripheral rods, and (3) the performance of weapons-grade mixed oxide fuel materials can be predicted with acceptable accuracy.

1.0 INTRODUCTION

The U.S. Department of Energy (DOE) is implementing a program to dispose of a portion of the nation's surplus weapons-grade (WG) plutonium by reconstituting it into mixed-oxide (MOX) fuel pellets and irradiating the fuel in commercial light water reactors. Accordingly, the DOE has contracted with Shaw AREVA MOX Services to qualify the fuel for batch irradiation. A formal plan has been developed to guide the fuel qualification process (Reference 1).

In accordance with the plan, four Mark-BW/MOX1 lead assemblies were supplied to Duke Energy's Catawba Nuclear Station, Unit 1, for irradiation starting in spring 2005. The assemblies were placed in high power but non-limiting locations that are expected to be representative of the batch peaking requirements. The first cycle of irradiation was completed in fall 2006, and the lead assemblies were examined at poolside. The second cycle was completed in spring 2008, and the assemblies were again examined at poolside. The fuel had achieved assembly average and maximum rod average burnups of 41.8 and 47.3 GWd/MThm, respectively. After the poolside examination, five fuel rods were removed from one assembly (MX03, also known as NJ13GG) and shipped to Oak Ridge National Laboratory for hot cell examination. The two cycles of irradiation, two poolside examinations, and hot cell examination complete the irradiations and examinations that are required for fuel qualification. The exams were designed to cover the full scope of standard fuel inspections and tests, and to provide the performance data needed for fuel qualification. The results of the examinations have been published in several reports (References 2, 3, and 4).

The purpose of the post-irradiation examinations was to provide performance data to confirm the assumptions and models that were used for design and analysis of the WG MOX lead assemblies. Accordingly, the purpose of this report is to compare the results of the postirradiation examinations (PIEs) with predictions and expectations, to demonstrate that the fuel provided acceptable performance, and to confirm that the performance of the WG MOX can be adequately predicted.

The primary focus of this report is on fuel pellet and fuel rod performance. Because the poolside examinations covered other parts of the fuel assemblies, there is also some discussion of the lead assembly design. A detailed description of the design has been published (Reference 5).

Figure 1-1 shows the general arrangement of the fuel assembly and specifies the nomenclature for spacer grids, mid-span mixing grids (MSMGs), and fuel rod spans.

1.1 Scope and Extent of Examinations

The scope and extent of the poolside exams are discussed in Reference 2.

Plans for the hot cell exams are outlined in Reference 5. The following considerations (Reference 5, supplemental question 5) were used in selecting rods:

At least four rods will be selected for hot cell examination. Rod selection will reflect the following considerations: (1) High-burnup rods are generally preferable. (2) The rods should be chosen from more than one assembly. (3) The rods should represent all three zones of plutonium content. (4) The rods should be chosen from various types of locations (e.g., corner, interior).

The actual selection of rods is shown in Figure 1-2. Comparison with the text above shows that the only consideration that was not satisfied was that the rods should be chosen from more than one assembly. Because the core design was quarter-core symmetric and the lead assemblies were in symmetric locations, there would have not been significant benefit to taking rods from multiple assemblies.

The actual scope and extent of the hot cell exams are discussed in References 3 and 4.

Table 1-1 provides a comparison of the scope and extent of the actual hot cell PIE to the examinations described in Reference 5. In most cases, the actual extent exceeds the planned extent, often by a substantial margin. Four rods were punctured in the hot cell. Because that was the minimum number to be examined, the measurements of gas pressure and void volume are sufficient, even though rod B-14 was not punctured. One reduction in scope from the plan is noted: Gallium analysis of archival fuel pellets has not been performed. Measurements on irradiated pellets plus archival and irradiated cladding are sufficient to show that gallium transfer from the fuel to the cladding does not threaten fuel rod integrity.

1.2 Organization of Report

Section 2.0 provides a summary of the broad conclusions. Section 3.0 discusses the results of the poolside examinations, and Section 4.0 discusses the hot cell examination. These are the largest sections, and a separate subsection is provided for each type of examination. Finally, Section 5.0 lists the references.

To guide the reader, Table 1-2 lists the in-reactor phenomena from the *Standard Review Plan* (SRP), Section 4.2 (Reference 6) and the examinations that provide information about each phenomenon. As is noted in the table, a few phenomena are not addressed because they (1) do not apply to pressurized water reactor fuel, or (2) are not relevant to qualification of MOX fuel. Spacer grid spring relaxation and guide tube wear fall into the second category because these components are not in contact with the fuel and will only be affected indirectly, such as by fast neutron fluence.

This report discusses and interprets the results of the postirradiation examinations. It is intended to provide information about MOX fuel materials rather than as a safety analysis of any given design. A safety analysis of the Mark-BW/MOX1 has been provided (Reference 5), and future MOX fuel is expected to use new designs.

Table 1-1—Extent of Hot Cell Examinations

| Inspection or Test | Planned Extent | Actual Extent |
|--|---|---|
| Visual examination | None specified | 5 rods |
| Fuel rod length | None specified | 5 rods |
| Gamma scanning | 2 rods | 5 rods |
| Eddy current testing | None specified | 5 rods |
| Fuel rod profilometry | None specified | 5 rods |
| Gas pressure, void volume, and gas analysis | All rods, 4 minimum | 4 rods |
| Optical microscopy of fuel and cladding | 8 sections, with cladding metallography and pellet ceramography on each | 9 sections, with cladding metallography and pellet ceramography on each |
| Transmission electron microscopy of cladding | None specified | 5 irradiated samples plus 1 archival sample |
| Scanning electron microscopy of fuel and cladding | None specified | 5 samples |
| Radial burnup profile | 2 samples | 5 samples |
| Burnup determination | None specified | 11 samples |
| Isotopic analysis of fuel | None specified | 11 samples |
| Gallium analysis of archival pellets | 1 sample minimum | None |
| Gallium analysis of irradiated pellets | 1 sample minimum | 3 samples |
| Gallium analysis of archival cladding | 1 sample minimum | 2 samples |
| Gallium analysis of irradiated cladding | 1 sample minimum | 5 samples |
| Cladding hydrogen analysis | None specified | 7 irradiated samples plus 2 archival samples |
| Expanding plug testing of cladding (room and elevated temperature) | 4 samples | (Tests are still in progress) |
| Axial tensile testing of cladding (room and elevated temperature) | None specified | (Tests are still in progress) |
| Pellet density | None specified | 5 samples |
| Inspection of wear marks | None specified | 1 rod survey plus 1 sample |
| Cladding surface microscopy | None specified | 1 sample |

Table 1-2—Applicability of Examination Results to SRP In-Reactor Phenomena

| SRP In-Reactor Phenomenon | Section Number and Examination |
|---|--|
| Fuel and burnable poison rod growth | 3.4 Fuel Rod Growth (Poolside Measurements) 4.2 Fuel Rod Growth (Hot Cell Measurements) |
| Fuel rod bowing | 3.2 Fuel Rod Visual Examinations (Poolside) 3.8 Water Channels 4.1 Fuel Rod Visual Examinations (Hot Cell) |
| Fuel rod and spacer grid oxidation and hydride levels | 3.1 Fuel Assembly Visual Examinations 3.2 Fuel Rod Visual Examinations (Poolside) 3.7 Fuel Rod Oxide Thickness 4.1 Fuel Rod Visual Examinations (Hot Cell) 4.7 Optical Microscopy of Fuel and Cladding |
| Fuel rod fretting | 4.1 Fuel Rod Visual Examinations (Hot Cell) 4.17 Inspection of Wear Marks |
| Fuel assembly growth | 3.3 Fuel Assembly Growth |
| Fuel assembly bowing | 3.5 Fuel Assembly Bow |
| Channel box wear and distortion | <i>(not applicable to pressurized water reactor fuel)</i> |
| Fuel rod ridging (PCI) | 4.5 Fuel Rod Profilometry |
| Crud formation | 3.2 Fuel Rod Visual Examinations (Poolside) 4.1 Fuel Rod Visual Examinations (Hot Cell) |
| Fuel rod integrity | 3.2 Fuel Rod Visual Examinations (Poolside) 4.1 Fuel Rod Visual Examinations (Hot Cell) 4.4 Eddy Current Testing |
| Holddown spring relaxation | 3.10 Holddown Spring Height 3.11 Holddown Spring Stiffness |
| Spacer grid spring relaxation | <i>(not relevant to qualification of MOX fuel)</i> |
| Guide tube wear characteristics | <i>(not relevant to qualification of MOX fuel)</i> |

Figure 1-1—General Arrangement of Mark-BW/MOX1 Lead Assembly

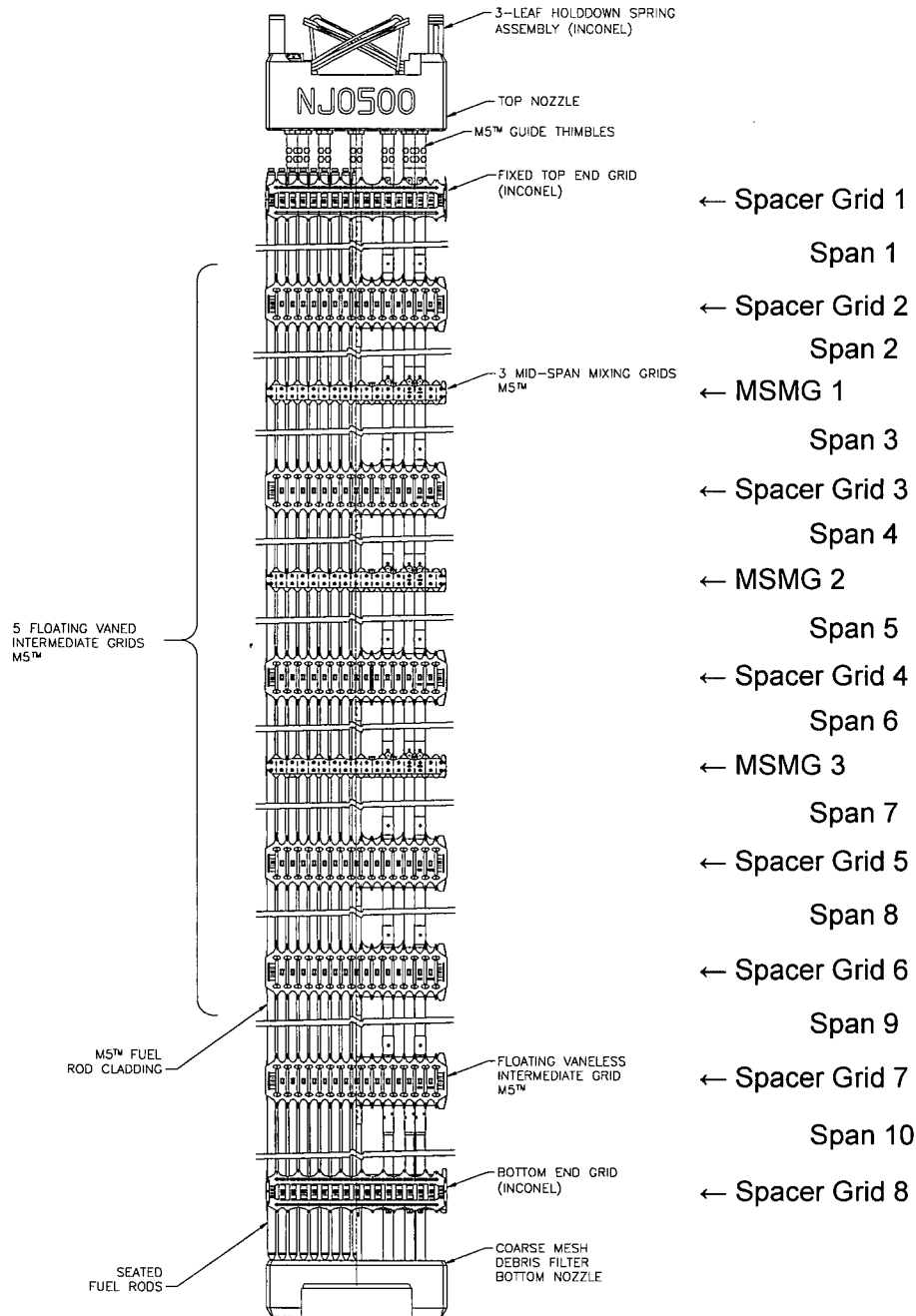
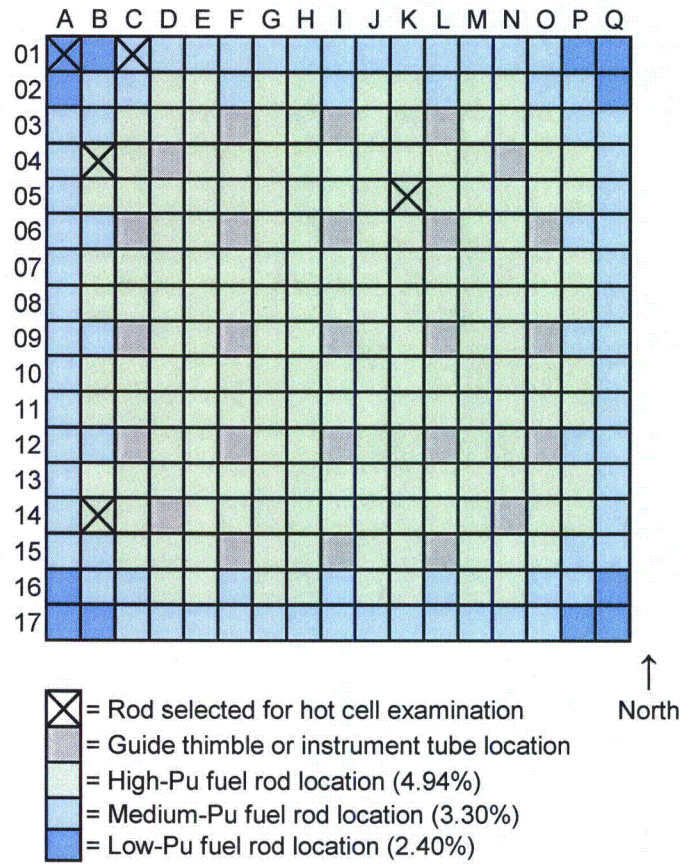


Figure 1-2—Locations of Rods Selected for Hot Cell Examination



2.0 SUMMARY AND CONCLUSIONS

Four lead assemblies containing WG MOX fuel pellets were manufactured, shipped to Duke Energy's Catawba Nuclear Station, Unit 1, and irradiated for two cycles. A basic poolside PIE was completed after the first cycle, and a more extensive poolside PIE was completed after the second. Five fuel rods were then removed from one assembly and shipped to Oak Ridge National Laboratory for hot cell examination. Together, the examination campaigns satisfy the PIE requirements and commitments as laid out in Reference 5.

This report summarizes and interprets the results of the PIEs and shows how the results are related to the fuel system design bases. To the extent possible, the results are compared with predictions or expectations. It is found that (1) the fuel provided acceptable performance, (2) future irradiations may benefit from more advanced neutronic methods that will reduce the uncertainty for peripheral rods, and (3) the performance of WG MOX fuel materials can be predicted with acceptable accuracy.

3.0 RESULTS OF POOLSIDE EXAMINATIONS

This section discusses and interprets the results (Reference 2) of the various poolside PIEs. A separate subsection is provided for each exam.

3.1 *Fuel Assembly Visual Examinations*

The faces of all four fuel assemblies were visually examined at poolside after each cycle of irradiation (Reference 2). The poolside exams provided video recordings that show the full length of all peripheral rods, the top and bottom nozzles, and the grids. Short sections of the guide thimble assemblies were visible at the shoulder gap. The appearance of the assemblies was expected to be similar to that of a low-enriched uranium (LEU) assembly (Reference 5, Table 8.1).

The fuel assemblies appeared to be in excellent condition. No mechanical damage to the grids was noted. The end grids had a bright appearance even after two cycles of irradiation, indicating that there was very little oxidation. The intermediate spacer grids and mid-span mixing grids had a slightly duller appearance, but the oxidation appeared to be quite light. The lightness of the oxidation is corroborated by the measurements of guide thimble oxide, which are reported in Section 3.9. The appearance of the oxide layer was normal, that is, comparable to what would be expected for LEU assemblies of similar burnups.

Although the assemblies had been ultrasonically cleaned before the exams, some of the grids had variations in luster that were attributed to areas of light crud (see, for example, Reference 2, Figure 4-10). The appearance was normal, that is, comparable to what would be expected for LEU assemblies of similar burnups. Because of the light oxidation, the level of hydriding was expected to be low.

No damage to the nozzles or guide thimble assemblies was noted.

The condition of the fuel rods is discussed separately in Section 3.2.

During reconstitution of assembly MX03, the top nozzle was removed and replaced. No difficulties were encountered in using the quick disconnect.

In summary, the appearance and condition of the fuel assemblies were similar to those of LEU fuel of comparable burnup, as expected. The fuel assembly visual examinations therefore indicated acceptable and predictable performance.

3.2 Fuel Rod Visual Examinations (Poolside)

The peripheral fuel rods of all four assemblies were visually examined at poolside after each cycle of irradiation (Reference 2). The poolside exams provided video recordings that show the full length of all peripheral rods. Selected fuel rods were examined again in a hot cell, as is discussed in Sections 4.1, 4.17, and 4.18. The appearance of the rods was expected to be similar to that of rods in an LEU assembly (Reference 5, Table 8.1).

In both poolside examinations, all of the fuel rods had a dark, uniform oxide layer that appeared to be tightly adherent. The appearance was consistent with light oxidation, and that observation was confirmed by the quantitative measurements discussed in Sections 4.7 and 4.9. The rods were free of significant crud deposits, but the assemblies had been ultrasonically cleaned before the exams, so any loose crud had presumably been removed. A slight mottling or “camouflage” appearance was noted in some locations after the second cycle of irradiation (Reference 2, p.4-2); that is normal for M5 cladding. Some fuel rod bowing was noted in the lower spans during poolside exams after the second cycle; see Section 3.8 for quantitative measurements. The poolside exams indicated that the fuel rods were in good condition and had maintained their integrity through two cycles of irradiation. Because of the light oxidation, the level of hydriding was expected to be low. See Section 4.13 for a discussion of hot cell measurements of hydrogen concentration in the cladding.

In summary, the appearance of the fuel rods was similar to that of LEU fuel of comparable burnup, as expected. The fuel rod visual examinations therefore indicated acceptable and predictable performance.

3.3 Fuel Assembly Growth

After each cycle, the lengths of all four fuel assemblies were measured and compared to the as-built lengths. The amount of growth was expected to be similar to that of LEU assemblies with M5 cladding and guide thimbles and with similar burnups (Reference 5, Table 8.1).

The measured amounts of growth varied from [] to [] inch at the end of the first cycle and from [] to [] inch at the end of the second (Reference 2, p. 4-10). The measurements indicated that the fuel assemblies had an axial clearance throughout their irradiation, that is, the holddown springs were never fully compressed.

One criterion for reinsertion of the assemblies for a third cycle was that the assembly growth not exceed [] inch. The assembly with the greatest amount of growth therefore exceeded the criterion by [] inch—less than the thickness of a dime. Because some of the assemblies did not meet the criterion for reinsertion, they were all discharged.

The amount of assembly growth after two cycles was slightly greater than expected, but an investigation determined that the MOX fuel was not the root cause of the higher assembly growth. Because there is now no intention to use the Mark-BW/MOX1 design, the results do not explicitly apply to future fuel assemblies.

In summary, the growth of MOX fuel assemblies can be acceptably predicted, and the amount of growth was acceptable for the level of irradiation to which the assemblies were exposed.

3.4 Fuel Rod Growth (Poolside Measurements)

Fuel rod growth in assemblies MX01 and MX02 was measured at poolside after each cycle of irradiation. The shoulder gaps for at least 16 peripheral rods of each assembly were measured. Fuel rod growth was then determined from the fuel assembly growth and the change in shoulder gap from the unirradiated condition to the irradiated condition. Selected fuel rods from assembly MX03 were also measured in a hot cell, as is discussed in Section 4.2. The amount of growth was expected to be similar to that of LEU fuel rods with similar burnups (Reference 5, Table 8.1).

MX03 and MX04 were evaluated by visual inspection. Video records showed that the shoulder gaps for these assemblies were comparable to those for MX01 and MX02. No unusually long fuel rods were seen in the fuel assembly videos. Because fuel rod failure and secondary hydriding often result in excessive fuel rod growth, the lack of any unusually long fuel rods is consistent with having maintained the integrity of the rods.

The results of the fuel rod growth measurements are shown in Figure 3-1 and compared with the LEU fuel rod database. The best estimate and tolerance limits are from an empirical model

that is used for mechanical design and predicts growth on the basis of fuel rod burnup. The amount of fuel rod growth as measured at poolside varied from [] to [] inch ([] to []%) at the end of the first cycle and from [] to [] inch ([] to []%) at the end of the second (Reference 2, pp. 4-12 and 4-13). All of the measurements at the end of the first cycle were well within the 95%/95% tolerance interval for LEU fuel rods, so it was concluded that the measured growth was as expected. At the end of the second cycle, [] found to be outside the 95%/95% tolerance interval for LEU fuel rods. However, the deviation from the prediction was modest, as can be seen from Figure 3-1. The minimum observed shoulder gap after two cycles was [] inch. This value is much larger than any deviation between the predictions and measurements, and it provides ample margin for fuel rod growth.

In summary, the growth of the MOX fuel rods was somewhat greater than that of LEU rods with similar burnups, and therefore somewhat greater than expected. However, the remaining shoulder gap was still so large that there is no concern about loss of shoulder gap. The accuracy of the prediction and the performance of the fuel rods are therefore both acceptable.

Figure 3-1—Comparison of MOX Fuel Rod Growth with Experience



3.5 Fuel Assembly Bow

Fuel assembly bow was measured on two adjacent faces of each fuel assembly. Measurements were taken after each cycle of irradiation. The amount of bow was expected to be similar to that of LEU assemblies with M5 cladding and guide thimbles and with similar burnups (Reference 5, Table 8.1).

The maximum displacement, as measured parallel to one face of the assembly, was about [] inch after the first cycle, and slightly smaller, about [] inch, after the second. The maximum magnitude of the displacement, as calculated from the measurements on two orthogonal faces, was [] inch after the first cycle and [] inch after the second (Reference 2, pp. 4-6, 4-7, 4-14, 4-15, and 4-35). All of these values are within the experience base for LEU fuel assemblies. The effect of assembly bow on control rod insertion depends not only on the magnitude of the bow but also on the number of times that the transverse displacement changes sign. “C-shaped” bows, for which the displacements are predominantly of one sign, are considered to cause the least resistance, whereas “S-shaped” and “W-shaped”

bows cause progressively more resistance. The larger bows in the MOX lead assemblies were predominantly C-shaped. Only one profile had a significant S-shaped character: [

]

Because of interaction between adjacent fuel assemblies, it is possible that a large region of a core or even an entire core could bow in one direction. However, the correlation of bows between the lead assemblies appeared to be weak or nonexistent. There may be a slight tendency for the fuel assemblies to bow toward the periphery of the core (Reference 2, p. 4-7).

In summary, the fuel assembly bow was similar to that of LEU fuel of comparable burnup, as expected (Reference 5, Table 8.1). Because the amount of bow was limited [

], fuel assembly bow is not expected to impede control rod insertion. Therefore, the fuel assembly bow performance was acceptable.

3.6 Spacer Grid Width

“Width” refers to the size of a spacer grid as measured perpendicular to the axes of the fuel rods. Before irradiation, all of the grids were measured in both the north-south and east-west directions. After two cycles of irradiation, widths were again measured on spacer grids 2 through 5 of assembly MX01 and spacer grids 1 through 5 of assembly MX02. (Nomenclature for grids is as shown in Figure 1-1.) The results of the as-irradiated measurements were compared to the as-built dimensions. The MOX fuel assemblies have Alloy 718 (UNS N07718) end grids and M5 intermediate spacer grids.

Because Alloy 718 and M5 have different growth characteristics, different predictions and expectations apply. The growth of the upper end grid (spacer grid 1) was expected [

]. Before the fuel assemblies were irradiated, it was predicted that the amount of growth for the intermediate grids would not exceed the upper tolerance limit, which was []% or [] inch for a maximum rod average burnup of 47.3 GWd/MThm (Reference 5, question 27). Although the latter prediction was called an “acceptance criterion” in Reference 5, the actual criterion for acceptable operation is that the grid width must not exceed the fuel assembly pitch, 8.466 inch.

The measured growth of the upper end grid (Reference 2, p. 4-16) was [] inch in one direction and [] inch in the other. This amount of growth is so small, and so much smaller than that of the intermediate grids, that it may be considered as [].

The amount of growth for the intermediate spacer grids varied from [] to [] inch for MX01 and [] to [] inch for MX02 (Reference 2, p. 4-16). The largest growth for an intermediate grid was reported as [] inch. That measurement and several others exceeded the upper tolerance limit by a small amount—less than the thickness of a sheet of paper. But the largest width for an intermediate grid was reported as [] inch, so all of the grids remained in compliance with the criterion for acceptable operation. No other width measurements are available for M5 grids in a Mark-BW-style assembly. However, the measurements on the MOX assemblies fell within the range of experience for LEU assemblies with Zircaloy-4 grids in high-burnup assemblies. Finally, it is noted that grid designs have been changed, and the new designs grow less.

In summary, the intermediate spacer grid growth was somewhat greater than was originally predicted, but it was similar to that of LEU fuel of comparable burnup. It also complied with the criterion that the grid width not exceed the fuel assembly pitch. Therefore, the spacer grid growth performance was acceptable.

3.7 Fuel Rod Oxide Thickness

After two cycles of irradiation, external fuel rod oxide thickness was measured at poolside by an eddy-current technique. The measurements were taken on selected rods of assemblies MX01 and MX02. The eddy-current coil was scanned over a length of about [] inches on each rod. [

] To avoid removing rods from the assembly, the measurements were taken only on peripheral rods.

The acceptance criterion for fuel rod oxidation was that the oxide thickness not exceed 50 μm (using a moving average over 1 inch) (Reference 5, Table 8.2). Two peripheral rods (A-01 and C-01 of assembly MX03) were included in the COPERNIC2 calculations for the lead assemblies. Because C-01 had one of the highest burnups for a peripheral rod, it was expected that the measured oxide thicknesses would not exceed the maximum predicted thickness for C-01, which was [] μm .

The largest individual measurement was [] μm (Reference 2, pp. 4-17 and 4-18). The average oxide thickness over the full length of all the scans was [] μm for MX01 and [] μm for MX02. [

] The measured oxide thickness was somewhat less than had been predicted.

As is discussed in Sections 4.7 and 4.9, hot cell measurements of oxide thickness confirmed the poolside measurements.

In summary, the fuel rod oxidation was in compliance with the acceptance criterion and was somewhat less than had originally been predicted. Because smaller oxide thicknesses correspond to greater margin, the difference between the predicted and measured values is not a concern.

3.8 *Water Channels*

At the end of two cycles of irradiation, water channel measurements were taken on all four assemblies. Water channel spacing is the distance between two adjacent rods (or a rod and an adjacent tube) in a fuel assembly at the mid-plane between spacer grids. These spacings can be classified as fuel-rod-to-fuel-rod (FR-FR), fuel-rod-to-guide-thimble, or fuel-rod-to-instrument-tube spacings. Water channel measurements were taken in two orthogonal directions at the mid-span planes of the assembly. The result of greatest interest is []; the values given below use this measure of fuel rod bow. Two additional results, [], were also reported (Reference 2, p. 4-19).

Figure 1-1 provides the nomenclature for grids and fuel rod spans. For assemblies MX01, MX02, and MX04, the bottom three spans were measured; for assembly MX03, all ten spans were measured. The structural spacer grids (i.e., the grids other than the mid-span mixing grids) have roughly equal spacing, but because of the mid-span mixing grids, there are six short spans (2 through 7) and four long spans (1, 8, 9, and 10). As expected, fuel rod bowing was well controlled in the short spans, [] (Reference 2, p. 4-19). Larger amounts of fuel rod bow were seen in the long spans. [

]

The acceptance criterion provided in Reference 5 (question 27) was that, [

] if

the assemblies are to be operated without a peaking penalty. The bow measurements indicate that the lead assemblies would have been subject to such a penalty. Additional criteria were subsequently imposed by the utility; [

] In each case, the measurements satisfied the utility's criteria, so the level of fuel rod bow was acceptable.

The Mark-BW/MOX1 design is the Advanced Mark-BW design with the LEU fuel rods replaced by MOX fuel rods, so similar fuel rod bow performance was expected for the two designs. The poolside measurements confirmed that expectation; levels of fuel rod bow for the Mark-BW/MOX1 were within the range of experience for Advanced Mark-BW at similar levels of burnup.

In summary, the lead assemblies would have been subject to a peaking penalty during their third cycle of operation, but the level of fuel rod bow was in compliance with applicable acceptance criteria and comparable to levels seen with LEU fuel.

3.9 Guide Thimble Oxide Thickness

After two cycles of irradiation, oxide thickness was measured on the interior surfaces of the guide thimbles. Measurements were made at various elevations in the four guide thimbles closest to the northeast, southeast, southwest, and northwest corners of the fuel assembly (Reference 2, Section 4.9.1). The largest oxide thickness measurement was [] μm . This thickness is similar to what has been measured in LEU fuel assemblies with M5 guide tubes.

Guide thimble oxidation normally does not limit fuel assembly performance, so no specific predictions of oxide thickness were made. Instead, a corrosion allowance was assumed for

structural analyses. The amount of oxidation was less than what was assumed, so the structural analyses are conservative. Because hydriding results from oxygen pickup during oxidation, the hydrogen content of the guide thimbles will also be well controlled.

In summary, the guide thimble oxidation was consistent with assumptions about fuel performance. The measurements therefore indicated acceptable performance.

3.10 *Holddown Spring Height*

Holddown spring height was defined as the difference in elevation between the top of the holddown spring and the level at which the tang of the spring enters the top nozzle. Holddown spring heights were measured after two cycles of irradiation for each spring pack on MX01 and MX02. The average heights, rounded to 0.01 inch, were [] inches for both MX01 and MX02 (Reference 2, p. 4-20), versus a nominal unirradiated free height of [] inches. Using the unirradiated free height is appropriate because assembly of the top nozzle may cause elastic deflection of the spring packs.

The spring measurements indicate that the change in spring height from the unirradiated condition to that after irradiation is [] inch. In contrast, the fuel assembly growth for the four lead assemblies varied from [] to [] inch (see Section 3.3). Because the assembly growth was greater than the spring relaxation, the deflection of the spring in core from its unloaded position was greater after two cycles of irradiation than at the beginning of life. In addition, the measured spring stiffness after two cycles was slightly greater than that at the beginning of life (see Section 3.11), so the holddown force was larger after two cycles than at beginning of life.

In summary, the holddown springs retained their ability to prevent assembly liftoff under applicable conditions. The measurements therefore indicated acceptable performance.

3.11 *Holddown Spring Stiffness*

The stiffness of the holddown springs was measured after two cycles of irradiation for all four lead assemblies. The measurements were made by [

] The average stiffness for the four assemblies was []

pounds/inch (Reference 2, p. 4-21), which is comparable to the nominal beginning-of-life value of [] pounds/inch. A reduction in spring stiffness corresponds to a reduction in holddown margin. But the stiffness measurements do not indicate a reduction in spring stiffness and therefore do not indicate a reduction in holddown margin.

In summary, and as has been discussed in Section 3.10, the holddown springs retained their ability to prevent assembly liftoff under applicable conditions. The measurements therefore indicated acceptable performance.

4.0 RESULTS OF HOT CELL EXAMINATIONS

This section discusses and interprets the results of the various hot cell PIEs. As in Section 3.0, a separate subsection is provided for each exam.

Predictions with the COPERNIC2 fuel rod performance code are provided in various sections below, and these predictions are affected by the end-of-life burnup and the power history. A notable result of the examinations was that the measured burnup of rod C-01 was larger than what was predicted by reconstruction (see Section 4.10). Therefore, the actual power history for C-01 must have differed from the prediction. Comparisons of measurements with calculations based on the predicted power history are helpful, but they leave open the question of whether similar results would be obtained if the calculations had been based on the actual power history. The approach taken in this document is that the COPERNIC2 calculations for rod C-01 were run twice, first with the power history predicted by reconstruction, and then with an adjusted power history that provides better agreement with the measured end-of-life burnup. The former calculations are referred to as “unadjusted”; the latter are referred to as “adjusted” and reflect a 12% increase in power and burnup. Results for the adjusted power history are denoted as “C-01 adj” or simply “adj” in the tables and figures. Section 4.6 provides a discussion of how the adjusted power history was developed.

4.1 Fuel Rod Visual Examinations (Hot Cell)

The five fuel rods selected from assembly MX03 were visually examined in the hot cell at Oak Ridge National Laboratory. The entire surface of the fuel cladding of each rod was examined and photographed with the Advanced Diagnostics and Evaluation Platform (ADEPT) (Reference 3, section 1.1). One rod (C-01) was examined and photographed twice. Digital photographs were taken at 45-degree increments of azimuthal angle and approximately 40-mm increments of elevation. The appearance of the rods was expected to be similar to that of rods in an LEU assembly (Reference 5, Table 8.1).

As expected, the rods were found to be in excellent condition, with no evidence of fuel rod failure. The appearance was similar to that seen at poolside: the rods had a dark, uniform oxide layer that appeared to be tightly adherent. Variations in color, such as the “camouflage” pattern noted in Section 3.2, were more difficult to distinguish in the hot cell than at poolside. Cladding corrosion appeared to be well controlled, and cladding collapse was not observed.

The hot cell examinations revealed a number of marks on the cladding that appeared to result from grid-to-rod fretting (Reference 3, pp. 7-8). Grid-to-rod fretting results from the cross-flow that occurs between fuel assemblies that have different levels of flow resistance; it is not related to the use of MOX fuel. The marks varied from a light stain to indications of apparent wear of the fuel cladding, and their elevations corresponded to the locations of spacer grid stops and midspan mixing grid dimples. The depths of the marks appeared to be small in comparison to the thickness of the cladding. Grid-to-rod fretting has been known to cause fuel rod failure in LEU fuel, but examination of such rods showed large marks that reproduced the shapes of the grid stops. In contrast, the wear marks on the MOX rods were smaller and irregular, as is typical of less severe fretting.

In an effort to obtain depth measurements, elastomeric replicas were made of some of the marks, and the replicas were measured outside the hot cell (Reference 3, pp. 7-8). The results from the replicas had poor repeatability, so the section of cladding that appeared to have the deepest wear marks was defueled for additional examination. That examination is reported and discussed in Section 4.17.

Because fuel rod bowing had been observed at poolside, the hot cell photographs were reviewed for indications of rod-to-rod fretting. No evidence of fretting or contact was found.

The hot cell exams revealed a large number of circumferential rings or bands where the surface was glossier than elsewhere (Reference 3, p. 6). Such bands had not been seen at poolside. Analysis of the spacing indicated that the bands were artifacts of handling in the hot cell, produced by rubbing against the support rollers or other surfaces of ADEPT when the rods were rotated. That conclusion was confirmed when rod C-01 was examined a second time and it was found that the appearance of the bands had changed.

In summary, the appearance of the fuel rods was similar to that of LEU fuel of comparable burnup, as expected, except that indications of modest grid-to-rod fretting were seen. The fuel rod visual examinations therefore indicated acceptable and predictable performance.

4.2 Fuel Rod Growth (Hot Cell Measurements)

The lengths of all five rods were measured in the hot cell. The amount of growth was expected to be similar to that of LEU fuel rods with similar burnups (Reference 5, Table 8.1).

Repeated length measurements were taken on all five fuel rods. Repeatability was excellent, with standard deviations of the length measurements varying from [] to [] mm (Reference 3, Tables 7 to 11). The irradiated lengths were compared with the as-built lengths. The measured amounts of fuel rod growth varied from [] mm ([]%) to [] mm ([]%) (Reference 3, Table 12). The results are plotted in Figure 3-1. As can be seen from the figure, the results of the hot cell measurements are as expected for all the rods, including rod C-01 with both the unadjusted and adjusted power histories.

Fuel rod growths were also calculated with COPERNIC2. For all the rods, including rod C-01 with both the unadjusted and adjusted power histories, COPERNIC2 predicts increases in rod length that are larger than what was measured. The discrepancy is comparable to those seen in the COPERNIC2 database (Reference 8, Figure 7-52). In addition, the primary requirement related to fuel rod growth is that a gap be maintained between the top nozzle and the upper ends of the fuel rods. Because the actual growth was less than that predicted by COPERNIC2, there is no concern about excessive fuel rod growth.

In summary, the hot cell measurements of MOX fuel rod growth were consistent with experience. The accuracy of the prediction and the performance of the fuel rods are both acceptable.

4.3 *Gamma Scanning*

All five rods were gamma scanned over their full length with ADEPT. It was expected that the axial dependence of the gamma intensity would be consistent with the axial burnup profile predicted by neutronic modeling.

Energy dispersive spectroscopy was used to measure gamma intensity in two energy ranges: 400 to 950 keV (low energy) and 1100 to 1600 keV (high energy). The low energy range corresponds to the predominant gamma energies for decay of fission products, whereas the high energy range corresponds to the predominant gamma energies for decay of ⁶⁰Co. Because the fission products are mostly in the fuel stack, the low energy scan provides a good picture of the stack. Conversely, ⁶⁰Co is presumed to be primarily in the plenum spring, and the high energy scan provides a good picture of the plenum spring. The concentration of fission products is proportional to the local burnup, so the low energy gamma scan provides a surrogate

measurement of the axial burnup profile. The results of the gamma scanning are provided in Reference 3.

Figure 4-1 through Figure 4-5 provide comparisons of the low energy gamma scans with the axial burnup profile that was calculated with CASMO-4/SIMULATE-3 MOX. Because of the difficulty of making an absolute prediction of the gamma intensity, the calculated burnup profile has simply been scaled to match the gamma scans. Figure 4-4 does not distinguish between the unadjusted and adjusted burnup profiles for rod C-01, because the adjusted burnup profile for rod C-01 would appear identical to the unadjusted profile.

As can be seen from the figures, the gamma intensity decreases slightly more steeply at the ends of the fuel stack than does the calculated burnup profile. But in light of the difficulty of making neutronic predictions for a mixed core, the burnup profile was in excellent agreement with the gamma intensity. Some local variations in the gamma intensity are present as expected:

- Slight reductions in gamma intensity can be seen at most of the pellet-pellet interfaces. These reflect the reduction in the amount of fuel, because of pellet dishes and chamfers, rather than a reduction in burnup. Larger reductions indicate the presence of small pellet-to-pellet gaps.
- There are increases in burnup (“reflector peaks”) at the extreme ends of the fuel stack as a result of improved thermalization at those locations. Because the linear power is low at these elevations, the peaks do not challenge the heat transfer capabilities of the rod.
- There are reductions in burnup at the grid elevations, primarily as a result of poorer thermalization at these locations.

One notable difference between the gamma intensity profile and the calculated burnup profile is the reduction in gamma intensity for rod C-01 at elevations of roughly 1300 to 1700 mm (span 8). A similar but much smaller feature may also be present for rod A-01 at elevations of roughly 800 to 1100 mm (span 9). These can be explained in terms of fuel distortion. Extra water near a fuel rod improves the neutron thermalization and thus increases local power. Similarly, power will decrease if there is less water near a fuel rod. The amount of water near a fuel rod is affected by fuel rod bow and, for peripheral rods, by the amount of space between adjacent fuel assemblies.

The water channels adjacent to rods A-01 and C-01 were measured at poolside. Rod A-01, span 9 and rod C-01, span 8 were found to have small water channels, and changes in power by several percent have been calculated for comparable rod displacements. As both A-01 and

C-01 are peripheral rods, they could also be affected by the width of the assembly-to-assembly gap, which is affected by the bow of the assembly relative to adjacent assemblies. It is therefore concluded that the variations in gamma intensity could be explained by fuel distortion. However, a quantitative determination of its effects on gamma intensity is not possible because a time-dependent record of fuel distortion during irradiation is not available.

Fuel stack lengths were determined from the gamma scans and compared with the measured as-built stack lengths. The measured stack growth was then compared to the stack growth predicted with the COPERNIC2 fuel rod performance code. For all the rods, including rod C-01 with both the unadjusted and adjusted power histories, COPERNIC2 predicts changes in stack length that are larger than what was measured. The largest discrepancy is comparable to the largest values in the COPERNIC2 database (Reference 8, Figure 6-11). As with fuel rod growth (Section 4.2), it is suspected that the difference in stack growth reflects different irradiation conditions. The only requirement related to fuel stack growth is that the plenum length be sufficient to accommodate the plenum spring. The plenum lengths are substantially greater than the solid height of the spring, so it was clear that the plenum length was sufficient to accommodate the spring.

It has been noted (Reference 3, p. 21 and Table 3) that the plenum spring might not fill the entire length of the plenum. Because the function of the plenum spring is to prevent the formation of stack gaps before the fresh fuel is inserted into a reactor, the shortness of the spring does not indicate that the spring has failed to perform its function.

The low-energy gamma scans revealed several stack gaps (Reference 3, Table 4). The largest gap was in rod C-01 at an elevation of about 733 mm. The width of the gap was estimated to be 2 to 3 mm, and that estimate was confirmed by examination of a longitudinal section of that portion of the rod. The number and sizes of the stack gaps in the MOX rods are within the range of those observed by neutron radiography of high-burnup LEU rods.

In summary, the hot cell measurements of MOX fuel rod growth were consistent with predictions and experience. The axial burnup profile was as predicted, and the stack gaps were within the range of experience. In addition, the plenum length was sufficient to accommodate the plenum spring.

Figure 4-1—Low-Energy Gamma Scan for Rod A-01



Figure 4-2—Low-Energy Gamma Scan for Rod B-04



Figure 4-3—Low-Energy Gamma Scan for Rod B-14



Figure 4-4—Low-Energy Gamma Scan for Rod C-01



Figure 4-5—Low-Energy Gamma Scan for Rod K-05**4.4 Eddy Current Testing**

All five rods were inspected for gross flaws with an encircling eddy-current coil (Reference 3, p. 55). As expected, no indications of flaws were observed.

A standard rod, used for eddy current calibration, was also examined. The standard had [

]. All of the features of the standard rod were observed. In contrast, the marks described in Section 4.1 were not detected, so they were evidently below the calibration/sensitivity limits of the eddy current apparatus and do not pose a threat to fuel rod integrity.

In summary, the eddy current testing indicated that there were no significant defects in the cladding.

4.5 Fuel Rod Profilometry

All five rods were examined by profilometry over essentially the full length of the rods, in two azimuthal directions denoted as 0 degrees and 90 degrees. Rod diameters were measured at

elevation increments of approximately 1 mm. Two profiles were measured simultaneously in two perpendicular directions. Diameter measurements are reliable for locations that are at least 150 mm from either end of a fuel rod. It was expected that the diameter profiles would be consistent with those predicted by the COPERNIC2 fuel rod performance code.

The data were processed as follows. The measuring stations for 0 and 90 degrees were offset axially. To obtain the diameter in both directions at nearly the same elevation, the two sets of measurements were offset by the appropriate number of steps, and the measurements for the two directions were averaged. The measurements were then smoothed by [

] The results of profilometry are shown in Figure 4-6 through Figure 4-10, along with the results of COPERNIC2 calculations for the rods. Measurements that considered questionable because they are too close to the end of a rod are plotted in red. Note that Figure 4-9 includes results for both the unadjusted and adjusted power histories for rod C-01.

The overall trends in the diameter profiles are consistent between the predicted and measured results. Both have relatively large diameters near the middle of the stack, where the burnup is high and solid swelling of the pellets strains the cladding. Toward the ends of the stack, the diameter first decreases, then increases. All of the measurements are smaller than the nominal diameter of the cladding. The reduction in diameter is as expected; the burnups are not large enough to produce a net increase in rod diameter.

The variations in diameter reflect the processes that affect the fuel rod. Because of the pressure of the primary coolant, the cladding creeps, and its diameter is reduced. Creep is partially driven by neutron flux, so creep is slower and the diameter is greater at the extreme ends of the rod, where the flux is low. The diameter would therefore be smallest in the central portion of the stack, where the flux is highest, were it not for swelling of the pellets. Except at the extreme ends, the cladding is in hard contact with the pellets at end of life, so the cladding diameter reflects the amount of pellet swelling. The amount of swelling is largest in the high-burnup region in the central portion of the stack. The interpretation above is supported by the lack of pellet ridges near the ends of rods, as can be seen, for example, in Reference 3, Figure 46.

Rod diameters were also calculated with COPERNIC2 for 17 elevations. Figure 4-6 through Figure 4-10 provide comparisons of the calculated and measured diameters. Agreement of

measured and predicted diameters to within [] μm is common, though larger differences have also been seen (Reference 8, Figures 7-3 to 7-19, 7-23 to 7-28, and 7-30 to 7-37). By this standard, the measurements for rods B-04, B-14, C-01, and K-05 are as predicted. For rod C-01, the calculated and measured diameters are in agreement with both the unadjusted and adjusted power histories. The measurements for rod A-01 are somewhat larger than expected, but the differences are still comparable to those from previous experience.

Three localized reductions in fuel rod diameter are discussed in Section 2.5 of Reference 3. Two of these (Reference 3, Figures 64 and 65) were at locations where the gamma scans indicated relatively large stack gaps. In both locations, the reductions in diameter were smaller than those seen at stack gaps in high-burnup LEU fuel rods. The greater reduction in diameter may reflect the longer irradiation time for the LEU fuel. None of the LEU rods failed, so it is apparent that the stack gaps and reductions in diameter in the MOX rods do not threaten their integrity. The reductions in diameter indicate that these stack gaps formed during irradiation, and the cladding subsequently crept into the gaps.

The third reduction in diameter (Reference 3, Figure 66) had an axial extent that roughly corresponded to the length of one pellet. Rotational profilometry revealed that the rod was ovalized at this location with a maximum ovality (defined here as the maximum diameter minus the minimum diameter) of about [] μm (Reference 3, Figure 78). The ovality may have resulted from a pellet that had slightly different properties or cracked in a pattern that allowed a fortuitously small crack volume. A gross pellet defect, such as a large chip, can be ruled out because the gamma intensity did not indicate a reduction in the amount of fuel at this elevation. For comparison, the ovality of high-burnup LEU fuel rods has been found to exceed [] μm in some locations, so ovalization does not threaten the integrity of the fuel rod.

In summary, the agreement between the predicted and measured results was acceptable, and the measurements were consistent with acceptable performance of the fuel rods.

Figure 4-6—Measured and Predicted Diameter Profiles for Rod A-01



Figure 4-7—Measured and Predicted Diameter Profiles for Rod B-04

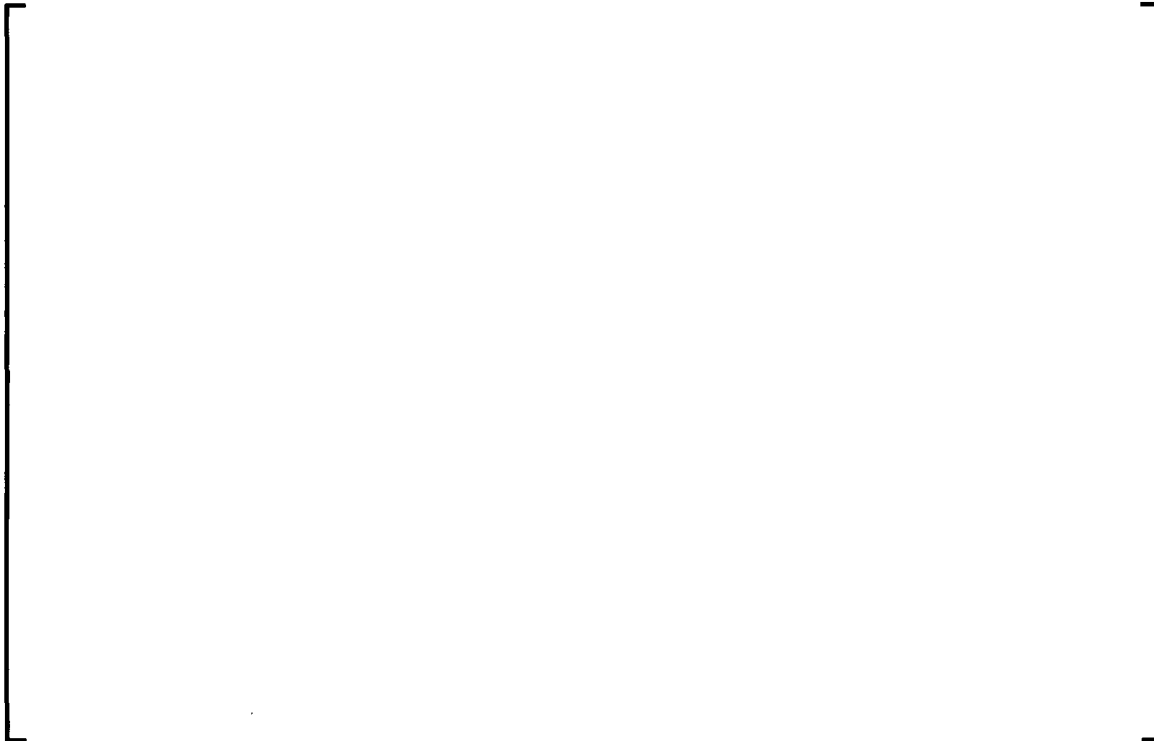


Figure 4-8—Measured and Predicted Diameter Profiles for Rod B-14



Figure 4-9—Measured and Predicted Diameter Profiles for Rod C-01



Figure 4-10—Measured and Predicted Diameter Profiles for Rod K-05**4.6 Gas Pressure, Void Volume, and Gas Analysis**

Rods A-01, B-04, C-01, and K-05 were punctured, and the gas pressure, void volume, and gas composition were determined (Reference 3). Rod B-14 was reserved as a spare. The expected result of the gas pressure and void volume measurements was that the gas pressure would be less than that predicted by the COPERNIC2 upper-bound model for fission gas release (Reference 5, supplemental question 5).

Four sets of COPERNIC2 calculations were performed:

- Calculations with the best estimate fission gas release model and unadjusted power histories were completed for all rods, and the results were compared with the measurements.
- The previous calculations were repeated with COPERNIC2's 95% upper bound model for fission gas release. These were used to determine whether the results were in agreement with expectations.
- Calculations with increased power and burnup were completed for rod C-01. These calculations used the best estimate model for fission gas release, but the linear power of

the rod was multiplied by a constant factor. Three different increases in power (and therefore in end-of-life burnups) were considered: []. The power history with an increase in burnup of [] provided the best agreement with the measured burnups reported in Section 4.10. It is denoted as "C-01 adj" or "the adjusted power history for rod C-01".

- Finally, the calculations with increased power were repeated with COPERNIC2's 95% upper bound model for fission gas release. These were used to determine the increase in burnup that would be needed to provide agreement with expectations.

Figure 4-11 and Figure 4-12 compare the measured and best estimate predicted values of void volumes and gas pressures, respectively. For rod C-01, best estimate predictions for both the unadjusted and adjusted power histories are shown. The measured pressures were adjusted to a temperature of 30 °C. All of the predicted void volumes were in excellent agreement with the measured volumes. Agreement to within $\pm 20\%$ between the measured pressures and best estimate predictions is generally considered acceptable. As can be seen from Table 4-1 and Figure 4-12, the poorest agreement was for rod C-01, for which the predicted best estimate value was about [] times the measured value. With the possible exception of C-01, agreement on pressure is considered to be acceptable. Further discussion of the adjusted power history for rod C-01 is provided below.

Table 4-1 lists the upper bound predictions of gas pressure. For all rods except C-01, the results were consistent with expectations because the measured pressure was less than the upper bound prediction.

The agreement between measurements and predictions would be improved if the power and burnup of rod C-01 were greater than predicted, and increasing the burnup in the COPERNIC2 calculations is appropriate because, as is discussed in Section 4.10, the measured burnups for C-01 were larger than predicted. Therefore, additional calculations were run with increased power and burnup. As was mentioned previously, the calculations were run for various burnup levels and with both the best estimate and upper bound models for fission gas release. The results are summarized in Table 4-2. It can be seen that for an increase in burnup of [] (C-01 adj), the upper bound prediction exceeds the measured pressure. That result is consistent with the result that the measured burnups for samples from rod C-01 are roughly [] to [] greater than the predicted values (see Section 4.10). It should be noted that in these calculations the power levels were simply multiplied by a scaling factor, and that other power histories could provide the same end-of-life burnups.

In summary, it is concluded that the predictions of void volume are consistent with the measurements for all of the rods and that the predictions of gas pressure are consistent with the measurements for all rods except C-01. But if the burnup of C-01 is adjusted to agree with the burnup measurements, the predicted gas pressure also agrees with the pressure measurements. The measured gas pressures are within the range of experience.

Table 4-1—Comparison of Measured and Calculated Gas Pressures



Table 4-2—Calculated Gas Pressure for Rod C-01 with Increased Burnup

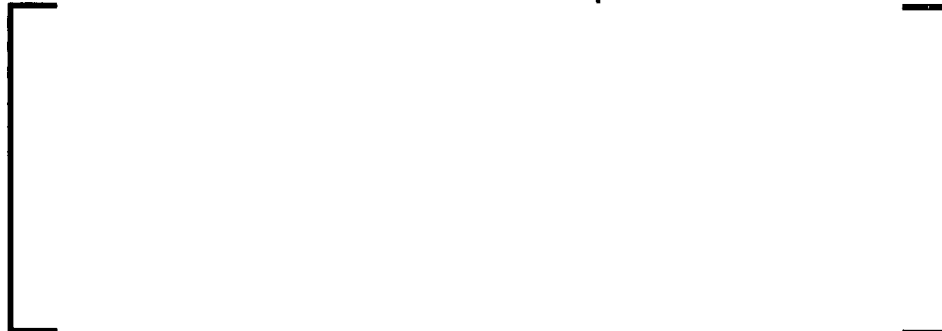


Figure 4-11—Measured and Predicted Void Volumes



Figure 4-12—Measured and Predicted Gas Pressures



4.7 *Optical Microscopy of Fuel and Cladding*

Nine metallographic samples were prepared and examined by optical microscopy. The results have been described and representative photomicrographs have been provided (Reference 4, Section 3.1). The work included three sets of examinations: (1) the entire sample in the as-polished state, (2) the fuel cladding, etched to reveal hydrides, and (3) the pellet, etched to reveal the microstructure. The examinations provided information on stack gaps, pellet cracking, pellet microstructure, water-side and fuel-side oxidation, hydrides, and reactions between gallium and the cladding.

The expected result was that the observations would be consistent with previous observations for reactor-grade MOX and LEU fuel.

Stack Gap

One metallographic sample was taken at the location where the gamma scans indicated the largest stack gap. Measurement of the photomicrograph indicated a gap length of [] mm. That value was within the range of experience for LEU fuel that had operated acceptably.

Pellet Cracking

The overall patterns of cracks in the fuel pellets were similar to those seen in reactor-grade MOX or LEU fuel. The results are therefore consistent with experience. One sample (see Reference 4, Figures 4 and 5) showed an unusual feature that resembles a contorted crack. A subsequent photograph (Reference 4, Figure 58), taken after the sample was repolished and etched, also shows a feature resembling a broad crack. Such features might conceivably appear if a thermal stress crack were nearly in the plane of the cross section. But because thermal stress cracks are typically rather straight, it may be more likely that there was a discontinuity in the pellet that resulted from contamination or shrinkage during sintering. In any case, the feature was localized and did not affect fuel rod performance.

Pellet Microstructure

The plutonium-rich agglomerates were visible in some photomicrographs of the as-polished specimens and of the etched specimens. The details of each photomicrograph reflect both the sample preparation and the local characteristics of the material, but the typical trends for MOX fuel are apparent: Near the cladding, the agglomerates contain many fine pores, and in some

cases, a “halo” of finer pores is visible at the perimeter. At mid-radius, the porosity in the agglomerates is coarser as a result of the higher fuel temperature. It was sometimes difficult to distinguish the agglomerates near the center of the pellets.

Microstructures similar to those shown in Reference 4 have been observed in reactor-grade MOX (see, for example, Figure 9 of Reference 9 and Figure 3 of Reference 10). The results for pellet microstructure are therefore consistent with experience and expectations.

The grain boundaries in the UO₂ matrix were not always readily visible, but when they were visible, the expected trend of smaller grains near the cladding and larger grains near the centerline was apparent.

The pellet specification (see Reference 1, Attachment D) imposes several requirements on the allowable sizes for plutonium-rich agglomerates. The largest agglomerates had a length of about [] μm (Reference 4, Figure 24); that result confirms compliance with the limit of 400 μm for a pure PuO₂ particle.

No evidence of centerline fuel melting was observed in the pellet microstructure. That result is consistent with requirements and is as expected for normal operation.

Water-Side Oxidation

Only one optical photomicrograph clearly showed the water-side oxidation of the cladding. The oxide thickness was roughly [] μm. Poolside measurements of oxidation for the same span give an average thickness of [] μm for MX01 and [] μm for MX02, so the results are in agreement. In contrast, COPENIC2 predicted an oxide thickness of [] μm for the nearest node, so the measured result is substantially less than predicted. (For C-01 adj, the predicted oxide thickness was [] μm at the nearest node.) Because smaller oxide thicknesses correspond to greater margin, the difference between the predicted and measured values is not a concern. Small oxide thicknesses have also been observed for M5 LEU fuel cladding and unfueled, irradiated M5 tubes (Reference 11, Table 3 and Figure 6). The oxide thickness is within the range of experience for LEU fuel.

For additional discussion of water-side oxidation, see Section 4.9.

Fuel-Side Oxidation

Fuel-side oxidation was visible in several high-magnification photographs. The clearest image of fuel-side oxidation is in Reference 4, Figure 19, which indicates a typical oxide thickness of about [] μm , possibly with a slight increase in thickness where an agglomerate is at the surface of the fuel pellet. It is difficult to determine the oxide thickness exactly from the optical photomicrographs. Scanning electron microscopy showed the oxide layer more clearly, so further discussion is deferred to Section 4.9. As is shown there, the results are consistent with experience.

Hydrides

Optical microscopy confirmed that the density and configuration of the hydrides were similar to those in LEU fuel. Representative photomicrographs of hydrides in cladding are provided in Reference 4, Figures 27 through 53. The hydriding is light, and the hydrides are discrete and predominantly circumferential. A few radial hydrides were noted; see, for example, Reference 4, Figures 32, 36, and 41. Similar hydrides have been observed in unfueled, irradiated M5 tubes (Reference 11, Figure 7) and in high-burnup M5 LEU fuel cladding.

Reaction between Gallium and Cladding

As expected, no evidence of a reaction between gallium and the cladding was seen in the optical photomicrographs of the inner surface of the M5 cladding.

In summary, all of the results of optical microscopy were consistent with experience and/or with acceptable performance of the fuel.

4.8 *Transmission Electron Microscopy of Cladding*

Samples for transmission electron microscopy were prepared from five sections of irradiated cladding and one section of archival cladding. The samples included four from the high-flux portion of the fuel rods plus one from the plenum of a fuel rod (low flux). Representative photomicrographs and the results of analysis were provided in Reference 4, Sections 6.1 through 6.1.10. The features that were characterized included grain size, β -Nb precipitates, *c*-component dislocation loops, *a*-component dislocation loops, radiation enhanced precipitates, and hydrides.

The primary mechanism by which MOX would affect the cladding is through fast neutrons, so it was expected that the structure of the cladding would be similar to that for LEU fuel with the same fast fluence.

Interpretation of the results of transmission electron microscopy has been provided in Reference 4, Section 6.1.10. The results were found to be consistent with those for M5 cladding on LEU fuel and for unfueled M5 tubes, so they are also consistent with acceptable performance of the fuel.

4.9 Scanning Electron Microscopy of Fuel and Cladding, Radial Burnup Profile

Five transverse samples of fuel and cladding from the high-flux regions of rods A-01, B-04, and C-01 were examined by scanning electron microscopy (Reference 4, Section 4.1). All of the samples were examined for general microstructure and for radial burnup profiles. Selected samples were also examined for water-side and fuel-side oxidation.

A separate sample of mechanically defueled cladding was examined for surface morphology and deposits; the results of that examination are provided in Section 4.18.

The expected result was that the observations would be consistent with previous observations for reactor-grade MOX and LEU fuel. The burnup profile was expected to be very irregular because of local variations in the initial plutonium content.

Pellet Microstructure

The microstructure of the fuel pellets was expected to be similar to that for reactor-grade MOX fuel, with numerous, small, plutonium-rich agglomerates scattered through the pellet.

The observed microstructure was consistent with expectations. Near the fuel-cladding interface, the agglomerates were visible as clumps of fine porosity, with pore sizes of a few micrometers (Reference 4, Figures 98, 102, etc.). Figure 98 of Reference 4 shows more pores in this region than do the other samples, and the pores are fairly uniformly distributed rather than clumped as would be expected with agglomerates. The microstructure therefore appears to show the beginning of a high-burnup rim structure in the matrix of the fuel. That result is consistent with a previous observation for a reactor-grade MOX sample (Reference 12, section 6.4) with a burnup of 44.5 GWd/MThm and a ^{235}U enrichment of 0.72%. For comparison, the lead assemblies had

a ^{235}U enrichment of []%, and a pellet-average burnup of [] GWd/MThm

(Reference 4, Table 51) near the sample shown in Figure 98 of Reference 4.

At mid-radius, the pores in the agglomerates were somewhat larger, as expected. Near the centerline, the agglomerates were difficult to distinguish. The large pores that develop in some MOX fuels (Reference 10, Figure 3, Centre; Reference 13, Figure 1, $r/r_o = 0.28$) were not seen; that result was consistent with the observations from optical metallography (Reference 4, Sections 3.1.1 and 3.1.3). As has been noted in Section 4.7, the structure of the WG MOX fuel is more like that shown in Figure 9f of Reference 9.

Water-Side Oxidation

It was expected that the thickness of the water-side oxide would be similar to that observed by optical microscopy (see Section 4.7) and eddy-current measurements (see Section 3.7). Oxide thicknesses were measured on three samples, and the average thicknesses were found to be [], [], and [] μm (Reference 4, Table 11, 12, and 13). For comparison, COPERNIC2 predicted oxide thicknesses of [], [], and [] μm , respectively, for the nodes closest to these samples. (With the adjusted power history for rod C-01, the predicted oxide thicknesses are [] and [] μm , respectively, for the nodes closest to the first two samples.) The photomicrographs (Reference 4, Figures 117, 118, and 119) show a thin, adherent, uniform oxide layer and confirm the excellent corrosion performance of the M5 cladding. The thicknesses observed by microscopy show less scatter than those measured by the eddy-current technique, though the average measurements are in good agreement.

The measured oxide thicknesses are much smaller than the licensing limit of 100 μm (Reference 14, Section 3.5 of Safety Evaluation Report).

Fuel-Side Oxidation

It was expected that the thickness and structure of the fuel-side oxide (or bonding layer) would be similar to that observed by optical microscopy (see Section 4.7). The observed thickness of the oxide layer was reported as “[] μm for the smooth portions of the bond layer” (Reference 4, Section 4.3). The distance from the metallic cladding to the deepest penetration of the bonding layer into the pellet was estimated to be about [] μm (Reference 4, Figure 121). Similar penetration depths have been seen in reactor-grade MOX and high-burnup LEU fuel. Scanning electron microscopy showed the fuel-

side oxidation much more clearly than optical microscopy did. The “fingered” structure at the interface between the fuel and oxide is similar to what has been seen previously in reactor-grade MOX (Reference 12, Figures 4 and 9) and high-burnup LEU fuel (Reference 15, Figures 18 and 26). Similarly, the current study and those cited above all found a comparatively smooth interface between the oxide and the unoxidized cladding. The results were therefore consistent with expectations.

For additional discussion of fuel-side oxidation, see Section 4.7.

Radial Burnup Profiles

For a MOX pellet with a homogeneous composition, the radial burnup profile would be expected to be nearly constant over much of the pellet, with a slight increase in burnup at the periphery, as is shown by the prediction in Figure 4-27 of Reference 8. However, the same figure also shows that the composition variations in MOX fuel produce large variations in the local burnup, which could mask any predicted trends.

The radial distribution of neodymium was determined by wavelength dispersive x-ray emission spectroscopy, and the results were provided in Section 4.4 of Reference 4. Unfortunately, the signal-to-noise ratio was very small. The noise is attributable to a background of gamma radiation at the detector, which was apparently not shielded adequately from the sample.

Burnup profiles were measured for all five samples. The extent of the examinations varied; each sample received at least two radial scans. Most of the scans showed an increase in the neodymium (or other lanthanide fission product) signal in the layers of fuel near the cladding, but it was not possible to quantify the change in burnup.

Two of the profiles do not appear to show an increase in the neodymium signal near the periphery of the pellet (Reference 4, Figures 126 and 130). The lack of a peak is attributed to a lack of agglomerates near the cladding that fall along the path of the scan. It is therefore concluded that the radial burnup profiles are consistent with expectations.

Reaction between Gallium and Cladding

As in the optical photomicrographs, no evidence for such a reaction was seen in the scanning electron photomicrographs of the inner surface of the M5 cladding. That result was as expected.

In summary, all of the results of scanning electron microscopy were consistent with experience and with acceptable performance of the fuel.

4.10 Burnup Determination

Burnup was determined by the ^{148}Nd method for 11 samples of fuel rod (Reference 4, Table 51). To provide information on the burnup profile, some of the samples were taken from near the ends of the fuel stack. Detailed isotopic analyses were also performed on the same samples, as is discussed in Section 4.11. The expected result was that the burnup measurements would be consistent with those predicted by neutronic modeling.

The neutronic analyses of the fuel assemblies provided two types of burnup results: the axial profile for the assembly as a whole and reconstructed rod averages. Because axial burnup shapes were not predicted on a rod-by-rod basis, the axial burnup profile for the assembly was scaled to match the reconstructed burnup of the rod in question.

The measured and predicted burnups are compared in Figure 4-13. It is apparent that the burnups are accurately predicted for all rods except C-01. However, adjustment of the power history as described in Section 4.6 brings the predictions (C-01 adj) into agreement with the measured values. It will be noted that C-01 is a peripheral rod and therefore was adjacent to an LEU fuel assembly. Because of the thermal neutron flux gradient at that location, the rod was subject to a larger uncertainty in its burnup prediction. Because the burnup calculation was performed by the utility rather than AREVA, the uncertainty cannot be quantified. Nevertheless, it is expected that future irradiations may benefit from more advanced neutronic methods that will reduce the uncertainty for peripheral rods.

At least one burnup sample was taken from the high-power portion of each rod. Because all the measured burnups were substantially smaller than 60 GWd/MThm, it is concluded that all of the rods were in compliance with the burnup limit (Reference 5, Section 4.0 of safety evaluation report).

In summary, burnups were accurately predicted for all rods except C-01, and it is expected that more advanced neutronic methods will reduce the prediction uncertainty for peripheral rods.

Figure 4-13—Measured and Predicted Burnups

4.11 Isotopic Analysis of Fuel

Detailed radiochemical analyses were performed on the 11 samples of fuel that were discussed in Section 4.10. The results included chemical analyses for Cs, Ce, Nd, Sm, Eu, Gd, U, and Pu, plus determinations of the isotopics of each of these elements (Reference 4, Tables 46 to 49). The expected result was that the elemental concentrations and isotopic abundances would generally follow the trends shown in the depletion calculations. Predictions were available only for the actinides, so only those results are discussed here.

There are two reasons that the depletion calculations should give results that differ from the results of the radiochemical analyses. First, the calculations were for a typical fuel design and irradiation, so they did not reflect the actual irradiation conditions for the lead assemblies. Second, the calculations provided assembly-average isotopics as a function of assembly-average burnup, whereas the radiochemical analyses provided the isotopics for the fuel in short rod samples. As a result, the radiochemical analyses were affected by the radial zoning of the plutonium concentration, the axial burnup profile, and variation in neutron flux and spectrum with position, whereas the calculated results reflect none of these. The depletion calculations are

used here because nothing else is currently available. More detailed neutronic calculations would be needed to better quantify the effects of neutronics on isotopics.

The depletion calculations do not account for radioactive decay after reactor shutdown, so the abundances of isotopes with half lives of less than 1000 years (^{238}Pu and ^{241}Pu) were corrected for radioactive decay. Production of ^{234}U by decay of ^{238}Pu was also accounted for. Decay of ^{242}Cm , ^{243}Cm , and ^{244}Cm to ^{238}Pu , ^{239}Pu , and ^{240}Pu , respectively, would also have occurred between the time of reactor shutdown and the time of analysis, but the concentration of curium was expected to be small, so the effects on plutonium concentration and isotopics would also be small.

The measured and calculated results are compared in Figure 4-14 through Figure 4-25. Figure 4-14 and Figure 4-15 show the mass fractions of U and Pu, expressed as grams of each element per gram of initial heavy metal (IHM). Figure 4-16 through Figure 4-25 show the isotopic abundances, expressed as mole percentages of the various isotopes for each element. The data markers indicate the rods from which the samples were taken. The results of chemical analysis are plotted against the measured ^{148}Nd burnup; the calculated values are plotted against the calculated assembly-average burnup. With the exception of Figure 4-16, each figure also includes the calculated assembly-average ("assembly calc") results from the depletion calculations. (The reported results from the depletion calculations did not include results for ^{233}U .)

Some of the dissolver solution from one sample was lost. As a result, there was not a clear relationship between the amount of heavy metal in the solution and that in the fuel sample, and the concentrations of the elements could not be plotted in Figure 4-14 and Figure 4-15. However, the isotopic abundances are not affected by the loss of solution, so those results are included in Figure 4-16 through Figure 4-25.

As expected, the measured results generally followed the predicted trends. The following comments apply:

- Because all the measurements in Figure 4-14 showed a U concentration that was greater than predicted, it appears that there was a slight positive bias in the U analyses.
- In many of the figures, the results fall into three bands: high-Pu (rods B-04 and K-05), medium-Pu (C-01), and low-Pu (A-01). From Figure 4-15 (total Pu concentration), it is seen that the initial amount of Pu directly affects the final amount.

- In the isotopic analyses, the differing results appear to reflect the neutron spectrum. The corner (A-01) and side (C-01) rods were next to LEU assemblies, so they received a larger thermal neutron flux than did the interior rods. As a result, ^{235}U was more strongly depleted in the peripheral rods, as is seen in Figure 4-18.
- The results for the interior rods are typically the closest to the assembly-average predictions. That is as expected because the majority of the rods are interior, high-Pu rods.
- ^{233}U was not detected in five of the samples, so these abundances are plotted as zero (Figure 4-16).
- The ^{234}U abundances are smaller than predicted, but the discrepancy is not of concern because the values are extremely low (Figure 4-17).

In summary, the differences between the measured and predicted values were reasonable, and the results of isotopic analysis were as expected. More detailed calculations would presumably give even better agreement.

Figure 4-14—Measured and Calculated Uranium Concentrations



Figure 4-15—Measured and Calculated Plutonium Concentrations



Figure 4-16—Measured ²³³U Abundances



Figure 4-17—Measured and Calculated ^{234}U Abundances



Figure 4-18—Measured and Calculated ^{235}U Abundances



Figure 4-19—Measured and Calculated ^{236}U Abundances



Figure 4-20—Measured and Calculated ^{238}U Abundances



Figure 4-21—Measured and Calculated ^{238}Pu Abundances



Figure 4-22—Measured and Calculated ^{239}Pu Abundances



Figure 4-23—Measured and Calculated ^{240}Pu Abundances



Figure 4-24—Measured and Calculated ^{241}Pu Abundances



Figure 4-25—Measured and Calculated ^{242}Pu Abundances**4.12 Gallium Analysis**

Gallium concentrations were measured in two samples of archival cladding, three samples of irradiated fuel, the cladding from the three fuel samples, and two samples of irradiated cladding from rod plenums (Reference 4, Section 7.1.3). The expected result was that there would be little gallium transfer from the pellets to the cladding, and that the gallium concentration in the cladding would remain low enough that the mechanical properties would not be affected.

Different studies have found different effects of gallium on cladding performance. Although metallic gallium and Ga_2O_3 have been found to be harmful to Zircaloy under certain conditions (Reference 16), no cladding degradation was seen when E-110 zirconium alloy was heated in contact with high-gallium MOX fuel pellets (Reference 17). Gallium has even been proposed as an alloying element for nuclear fuel cladding, at concentrations up to 1 weight percent (Reference 18).

Irradiation of the lead assemblies was preceded by irradiation of test rodlets in the Advanced Test Reactor. The rodlets contained WG MOX fuel that was prepared by a different process. Fuel pellets from test rodlets irradiated to 50 GWd/MThm have been analyzed, with irradiated

gallium concentrations of roughly 2320 to 6000 ng Ga / g oxide being reported (Reference 19, Table 6.5; Reference 20, Table 6.4). Examination of the test rodlets indicated no abnormal behavior of either the fuel or cladding.

The reported gallium concentrations in irradiated pellets from the lead assemblies were less than [] ng Ga / g oxide, or an order of magnitude smaller than that in pellets from the test rodlets. Therefore, the concentration of gallium in the fuel pellets is not a concern.

Analyses of the cladding provide additional assurance that gallium is controlled. The archival cladding samples contained very low gallium concentrations, less than [] ng Ga/ g metal. The fuel cladding adjacent to the pellets had gallium concentrations that varied from [] to [] ng Ga / g oxide. The increase in concentration indicates that some gallium transfer from the pellets to the cladding has occurred. However, the resulting concentration is smaller than the typical historical value of 275 ng Ga / g metal for Zircaloy-4 (Reference 5, Section 3.2.2 and Table 3.4). Therefore, the concentration of gallium in the fuel cladding is not a concern.

The cladding samples from the plenum had smaller gallium concentration than the cladding samples from the fuel stack. Therefore, gallium transport to the plenum in response to axial temperature gradients is not a concern.

In summary, the gallium measurements indicated that gallium concentrations and gallium transport are not a concern. That result is consistent with results of microscopy, which showed no effects of gallium on the cladding.

4.13 Cladding Hydrogen Analysis

Hydrogen concentrations were measured in four samples of archival cladding and seven samples of irradiated fuel cladding (Reference 4, section 7.1.2). One of the irradiated cladding samples was from the plenum of rod B-04. The expected result was that the hydrogen concentrations in the archival cladding would be in compliance with the specification and that concentrations in the irradiated cladding would be consistent with predictions from COPERNIC2.

The first two archival cladding samples were not cleaned before analysis. Because of the possibility that they were contaminated with oil or other hydrogenous materials, the results are considered to be invalid. All of the remaining samples were cleaned with acetone before

analysis. The valid archival samples had hydrogen concentrations of [] and [] $\mu\text{g H / g metal}$ (Reference 4, Table 28). These values are in compliance with the cladding specification, which allows up to [] $\mu\text{g H / g metal}$.

Table 4-3 provides a comparison of the measured and predicted hydrogen concentrations for the irradiated cladding samples. The measured hydrogen concentrations are generally lower than the predicted concentrations. Because lower hydrogen concentrations correspond to greater margin, the difference between the predicted and measured values is not a concern. That the hydrogen concentrations are lower than predicted is consistent with the observation in sections 4.7 and 4.9 that the water-side oxide thickness is less than predicted.

The agreement with Reference 21, Figure 5 is better, with most of the measurements falling near the bottom of the range shown in the reference. The data in the reference are presumably from the high-temperature portions of fuel rods, so a comparison of Table 4-3 with Reference 21 should exclude samples CHA-A-01-145-150, CHA-B-04-145-150, and CHA-B-04-3785-3790, which are from low-temperature locations.

In summary, the hydrogen analyses were consistent with experience and with acceptable performance of the fuel.

Table 4-3—Hydrogen Concentrations for Irradiated Cladding

NOTE: N/A = not applicable because COPERNIC2 does not report hydrogen concentrations for the plenum
In the sample identifiers, "CHA" denotes "cladding hydrogen analysis". That designation is followed by the rod identifier and then the elevation of the bottom and top of the sample, in millimeters, relative to the bottom of the lower end cap.

4.14 Mechanical Testing of Cladding: Expanding Plug

This examination will be discussed in a later revision of this report.

4.15 Mechanical Testing of Cladding: Axial Tensile

This examination will be discussed in a later revision of this report.

4.16 Pellet Density

Two attempts were made to measure the density of the fuel pellets (Reference 4, Section 5.1). In the first attempt, the fuel broke into fine fragments that were unsuitable for density measurements. The fuel was handled more gently in the second attempt, and larger fragments were obtained. The densities of five samples of irradiated fuel were measured by immersion in Fluorinert™ FC-43 Electronic Liquid. The expected result was that the measured pellet densities would be consistent with predictions from COPERNIC2.

Table 4-4 provides a comparison of the measured and predicted densities for the irradiated fuel samples. The results are expressed as fractional densities, that is, the actual density divided by the theoretical density, and the measured values in Table 4-4 are unweighted means of the values in Reference 4, Table 16.

The statistical errors (predicted minus measured values) given in Table 4-4 seem to have a slight bias; the measured values are consistently lower than the predicted values. Such a bias might result from the use of different immersion fluids (e.g., Fluorinert, water, bromobenzene) that differ in density and may also differ in their ability to wet fine porosity. Another source of bias might apply to the samples from rod C-01: the difference between the measured and predicted burnups (see Section 4.10) would affect fuel swelling and density. Densities for samples from rod C-01 were calculated for both the unadjusted and adjusted power histories. As can be seen in Table 4-4, the results for the adjusted power history are in better agreement with the measurements.

The errors in Table 4-4 are comparable to those in the COPERNIC2 database, so the measurements are considered to be consistent with predictions. The measured densities fall within the range of experience.

In summary, the density measurements were consistent with experience and with acceptable performance of the fuel.

Table 4-4—Fractional Density of Irradiated Fuel

NOTE: Error = Predicted minus Measured
In the sample identifiers, “PDF” denotes “pellet density fuel”. That designation is followed by the rod identifier and then the elevation of the bottom and top of the sample, in millimeters, relative to the bottom of the lower end cap.

4.17 Inspection of Wear Marks

As was noted in Section 4.1, wear marks were noted during the visual examinations. Instruments for characterizing wear marks were not available in the hot cell, so depth measurements were obtained by “replication”, that is, by applying an elastomeric resin to the mark, allowing it to cure, and removing the solidified replica. The replica was then removed from the hot cell, and the wear depth was determined by optical methods.

There were two attempts at replication. The first attempt was made during the nondestructive examination and covered a large number of marks on rod A-01 (Reference 3, Section 2.1.3 and Table 2). The largest depth measurements corresponded to some of the marks that had been judged to be the most severe on the basis of the visual exams, but it was not possible to make a quantitative correlation between the measured depth and the appearance. Duplicate replicas were made of a few marks, and reproducibility was poor.

Because of concerns about the reproducibility of the replication method, a 70-mm section of cladding with some of the most severe wear marks was cut from rod A-01 and defueled for closer examination (Reference 4, section 6.2). [

] It was hoped that defueling would reduce the radiation field to the point that the cladding could be removed from the hot cell. Although defueling undoubtedly

reduced the radiation field, the sample was still too radioactive, and a second campaign of replication was undertaken, this time with an improved technique. The results were still inconclusive. The investigators at Oak Ridge called the measurements “qualitative” and said that the results “cannot be considered reliable”.

Because the results from the replicas were inconclusive, the marks were compared to other wear marks that had been inspected at poolside. Examinations of LEU fuel have shown wear marks and fuel rod failures that were attributed to grid-to-rod fretting. [

] The LEU

rods showed large marks that reproduced the shapes of the grid stops, but the wear marks on the MOX rods were smaller and irregular, as is typical of less severe fretting. On this basis it is concluded that the fuel gave acceptable performance and that the wear marks are within the range of experience.

It is noted that grid-to-rod fretting is unrelated to the use of MOX and that future MOX assemblies are expected to use a different grid design that is more resistant to grid-to-rod fretting.

In summary, the appearance of the wear marks was consistent with experience and with acceptable performance of the fuel.

4.18 Cladding Surface Microscopy

One sample of cladding from near the top of the fuel stack of rod C-01 was mechanically defueled and examined by scanning electron microscopy (Reference 4, Section 4.5). The expected result was that the appearance of the surface would be similar to that of other M5 tubing exposed inside a reactor.

Some variations in appearance had been noted while the fuel was in the spent fuel pool (see Section 3.2) and to a lesser degree in the hot cell (see Section 4.1); such variations are common for M5 cladding. Under scanning electron microscopy, the variations were not visible. The oxide layer appeared tight and uniform with occasional light, particulate deposits of a foreign material (Reference 4, Figures 134 and 135). Wavelength-dispersive x-ray emission spectroscopy showed that the deposits contained iron, but other elements could not be detected

because of a low signal-to-noise ratio. Similar iron-containing deposits have been noted on guide tubes. The source of iron is presumably products of corrosion from the primary loop.

A few light, longitudinal scratches were observed on the cladding; these are presumably from handling or assembly (Reference 4, Figures 136 and 137). Because of the narrowness of the scratch, it was concluded that the scratch did not violate the specification for fresh cladding and therefore does not have a significant effect on fuel rod performance. By the same argument, it is concluded that the scratch is within the range of experience.

In summary, the appearance of the cladding was normal. It was consistent with experience and with acceptable performance of the fuel.

5.0 REFERENCES

1. DCS-FQ-1999-001, Rev. 4, *Fuel Qualification Plan*, July 2008.
2. ANP-10280P, Rev. 2, *Poolside Postirradiation Examination of MOX Lead Assemblies*, April 2009.
3. ORNL/MD/LTR-332, *MOX PIE Fuel Rod Examination Quick Look Report*, December 2009.
4. ORNL/MD/LTR-352, *MOX PIE Fuel and Clad Examination Final Report*, December 2011.
5. BAW-10238PA, Rev. 1, *MOX Fuel Design Report*, July 2004.
6. NUREG-0800, *Standard Review Plan*, Section 4.2, *Fuel System Design*, Revision 3, March 2007.
7. BAW-10147P-A, Rev. 1, *Fuel Rod Bowing in Babcock & Wilcox Fuel Designs*, May 1983.
8. BAW-10231P-A, Rev. 1, *COPERNIC Fuel Rod Design Computer Code*, January 2004.
9. Wolfgang Goll, Hans-Peter Fuchs, Reiner Manzel, and Fritz U. Schlemmer, "Irradiation Behavior of UO₂/PuO₂ Fuel in Light Water Reactors", *Nuclear Technology*, vol. 102, pp. 29-46, 1993.
10. Y. Guérin, J. Noirot, D. Lespiaux, C. Struzik, P. Garcia, P. Blanpain, and G. Chaigne, "Microstructure Evolution and In-Reactor Behaviour of MOX Fuel", *Proceedings of International Topical Meeting on Light Water Reactor Fuel Performance* (Park City, UT, USA, April 10-13, 2000), pp. 706-719.
11. Philippe Bossis, Bénédicte Verhaeghe, Sylvie Doriot, Didier Gilbon, Valérie Chabretou, Agnès Dalmais, Jean-Paul Mardon, Martine Blat, Alain Miquet, "In PWR Comprehensive Study of High Burn-Up Corrosion and Growth Behavior of M5® and Recrystallized Low-Tin Zircaloy-4", *Journal of ASTM International*, vol. 6, No. 2, Paper JA101314 (2009)

12. C. T. Walker, W. Goll, and T. Matsumura, "Further Observations on OCOM MOX Fuel: Microstructure in the Vicinity of the Pellet Rim and Fuel-Cladding Interaction", *Journal of Nuclear Materials*, vol. 245, pp. 169-178 (1997)
13. C. T. Walker, W. Goll, and T. Matsumura, "Effect of Inhomogeneity on the Level of Fission Gas and Caesium Release from OCOM MOX Fuel During Irradiation", *Journal of Nuclear Materials*, vol. 228, pp. 8-17 (1997)
14. BAW-10227P-A, Rev. 1, Evaluation of Advanced Cladding and Structural Material (M5) in PWR Reactor Fuel, June 2003.
15. J. Noirot, L. Desgranges, and J. Lamontagne, "Detailed Characteristics of High Burn-Up Structures in Oxide Fuels", *Journal of Nuclear Materials*, vol. 372, pp. 318-339 (2008)
16. ORNL/TM-13505, *Interactions of Zircaloy Cladding With Gallium: 1997 Status*, November 1997.
17. O. A. Alekseev, F. G. Reshetnikov, and V. A. Volkova, "Compatibility of Fuel-Element Cladding Materials with Gallium-Containing Uranium and Uranium-Plutonium Oxide Fuel", *Atomic Energy*, vol. 106, pp. 334-342 (2009)
18. U.S. Patent 5122334, "Zirconium-gallium alloy and structural components made thereof for use in nuclear reactors"
19. ORNL/MD/LTR-279, vol. 1, *MOX Test Fuel 50 GWd/MT PIE: Capsules 6 and 12 Final Report*, September 2005.
20. ORNL/MD/LTR-280, vol. 1, *MOX Test Fuel 50 GWd/MT PIE: Capsule 5 Final Report*, September 2005.
21. J. P. Mardon, G. L. Garner, and P. B. Hoffmann, "M5® a breakthrough in Zr alloy", *Proceedings of 2010 LWR Fuel Performance/TopFuel/WRFPM* (Orlando, Florida, USA, September 26-29, 2010)